Short Melamine Fiber Filled Nitrile Rubber Composites

R. S. Rajeev,[1] Anil K. Bhowmick,[1] S. K. De,[1] S. Bandyopadhyay[2]

[1]*Rubber Technology Center, Indian Institute of Technology, Kharagpur-721 302, West Bengal, India*
[2]*School of Materials Science and Engineering, The University of New South Wales, Sydney-2052, Australia*

Received 6 June 2002; accepted 8 January, 2003

ABSTRACT: This article reports the development of a new composite based on acrylonitrile butadiene rubber (NBR) and melamine fiber. Atomic force microscopy (AFM) and scanning electron microscopy (SEM) have been used to study the effect of a dry bonding system in improving the adhesion between the fiber and the matrix. Mechanical properties of the composites are improved in the presence of the dry bonding system comprising of resorcinol, hexamethylene tetramine (hexamine), and hydrated silica. SEM and atomic force microscopic (AFM) images show that there are distinct changes in the fiber-matrix interphase with the incorporation of the dry bonding system. A strong attachment of the fiber to the matrix is found in the SEM photomicrographs of the tensile fracture surfaces of the composites containing the dry bonding system. AFM section analysis and surface plot show that the improvement in tensile strength and modulus in the presence of the dry bonding system is due to the formation of a well-defined interphase between the fiber and the matrix. The width of the interphase between the fiber and the matrix is increased in the presence of the dry bonding system, which is reflected in the mechanical properties and aging characteristics. © 2003 Wiley Periodicals, Inc. J Appl Polym Sci 90: 544–558, 2003

Key words: short melamine fiber; nitrile rubber; composites; dry bonding system; physical properties; scanning electron microscopy; atomic force microscopy

INTRODUCTION

Short fiber reinforced rubber composites offer a great advantage over traditional composites in the relative ease in manufacturing and processing operations.[1–5] In comparison with composites having particulate fillers, a short fiber reinforced system possesses a high degree of reinforcement even at relatively low fiber content.[6] Melamine fiber has been labeled as a high performance fiber and possesses excellent heat and flame resistance.[7,8] Recently, the reinforcement of ethylene propylene diene rubber (EPDM) rubber by short melamine fiber has been reported.[9] In short fiber-rubber composites, the degree of reinforcement greatly depends on the nature of fiber, rubber, and fiber-matrix compatibility. Thus the chemical structures of both the fiber and the matrix and the presence of a bonding system determine the extent of interfacial adhesion, and thus the strength of the composites.[4] Previous studies on short melamine fiber reinforced rubbers have shown that the strength and the modulus of the composite are increased when the matrix is changed from EPDM rubber to a modified EPDM (that is, maleated EPDM rubber).[10] This observation leads to the choice of a polar rubber such as nitrile rubber (NBR) as the matrix. This article reports the results of studies on rubber-fiber composites based on nitrile rubber and melamine fiber. Scanning electron microscopic (SEM) and atomic force microscopic (AFM) studies have been carried out to study the morphological changes on the matrix and the fiber surfaces and at the fiber-matrix interphase with the incorporation of a dry bonding system to the melamine fiber filled nitrile rubber compound. Though AFM is widely used in the field of polymers,[11–18] there are only a few reports available on the use of AFM in the studies of short fiber filled rubber composites.[9,10,19] Since the dry bonding system comprising resorcinol, hexamine, and silica is known to provide effective reinforcement to elastomeric matrices filled with short fibers,[4,5,20–22] the same system has been chosen in the present study.

Correspondence to: S. K. De (skde@rtc.iitkgp.ernet.in).

Journal of Applied Polymer Science, Vol. 90, 544–558 (2003)

EXPERIMENTAL

Preparation of the composites

The details of the materials used and their characteristics are given in Table I. Formulations used for the preparation of the composites are given in Table II. It has been shown that resorcinol, hexamine, and silica normally in the ratio of 5:3:10 parts by weight provide optimum processing and mechanical properties of the short fiber filled rubber compositions.[5] However, for the short melamine fiber reinforced EPDM and maleated EPDM rubber composites, a higher concentration of resorcinol, hexamine, and silica (that is, resorcinol, hexamine, and silica in the ratio of 10:6:15 parts

TABLE I
Details of Materials Used and Their Characteristics

Material	Properties	Supplier
Nitrile rubber	Acrylonitrile content, 33% Mooney viscosity, ML (1 + 4) 120°C, 31	JSR Corporation Tsukiji Chuo-ku, Tokyo, Japan
Melamine fiber (trade name, BASOFIL)	Tenacity, 2.0 g/denier Elongation at break, 18% Density, 1.40 g/cc Maximum use temperature, 370°C Fiber length, variable Fiber diameter, 12–16 μm	BASF South East Asia Pte Ltd., Singapore
Resorcinol	Laboratory grade Density, 2.36 g/cc	E Merck, Mumbai, India
Hexamethylene tetramine (Hexamine, also known as Hexa)	Laboratory grade Density, 1.33 g/cc	S.d. Fine Chemicals, Boisar, Thane, India
Precipitated silica (trade name, Vulcasil S)	Density, 2.00 g/cc	Bayer AG, Leverkusen, Germany
Zinc oxide (ZnO)	Density, 5.57 g/cc	E-Merck, Mumbai, India
2, Mercaptobenzothiazole (MBT)	Density, 1.50 g/cc	ICI India Ltd., Rishra, India
Tetramethyl thiuram disulfide (TMTD)	Density, 1.40 g/cc	ICI India Ltd., Rishra, India
Sulfur	Density, 2.07 g/cc	S.d. Fine Chem, Mumbai, India

by weight) is needed.[9,10] Results of preliminary studies in the present system (not shown) show that resorcinol, hexamine, and silica in the ratio of 10:6:5 parts by weight provide optimum processing and mechanical properties. The terminology used to define the various formulations is as follows: N stands for nitrile rubber; B denotes the dry bonding system; and F stands for melamine fiber. The letter B is followed with subscript 0 when no dry bonding system is present in the matrix. The subscript accompanying the letter F indicates parts per hundred rubber (phr) of the fiber in the compound. As an example, the mix designation NBF_{10} represents the NBR compound containing the dry bonding system (that is, resorcinol/hexamine/silica in the ratio of 10:6:5 parts by weight) and melamine fiber at 10 phr.

The master batches were prepared by mixing the ingredients in a Brabender Plasticorder, model PLE-330 at 80°C and at a rotor speed of 30 rpm. The ingredients were added in the following order: rubber, zinc oxide, stearic acid, antioxidant, resorcinol, silica, fiber, and hexamine. Melamine fiber, which was in the pulp form, was separated manually and added in small increments in order to obtain uniform dispersion. After incorporation of the ingredients was over, the rotor speed was increased to 60 rpm and mixing continued for an additional 3 min. Then the hot material was taken out, sheeted out in a two-roll mill, and

TABLE II
Formulation of the Mixes

	Mix Designations					
Ingredients	NB_0F_0	NBF_0	NB_0F_{10}	NBF_{10}	NBF_{20}	NBF_{30}
NBR	100	100	100	100	100	100
ZnO	5	5	5	5	5	5
Stearic acid	1	1	1	1	1	1
Antioxidant[a]	1	1	1	1	1	1
Resorcinol	0	10	0	10	10	10
Hexamine[b]	0	6	0	6	6	6
Silica	0	5	0	5	5	5
Fiber	0	0	10	10	20	30
MBT[c]	1.5	1.5	1.5	1.5	1.5	1.5
TMTD[d]	1	1	1	1	1	1
Sulfur	1.5	1.5	1.5	1.5	1.5	1.5

[a] Polymerized 2,2,4-trimethyl 1,2-dihydroquinoline.
[b] Hexamethylene tetramine.
[c] 2-Mercaptobenzothiazole.
[d] Tetramethyl thiuram disulfide.

cooled. For the determination of mechanical properties, sheets having dimension of 145 mm × 120 mm × 2 mm were cured in a hydraulic press at 150°C under 5 MPa pressure by keeping the blank between two Teflon sheets in a compression mould.

Final batches of the compounds were prepared in the laboratory two-roll mill at a friction ratio of 1:1.2. The compounds were then rolled along the milling direction for four to five times and re-sent through the mill in order to obtain maximum fiber orientation in the milling direction. Sheets were then cured at 150°C for their optimum cure times, determined using a Monsanto Moving Die Rheometer (model MDR 2000). The Mooney viscosity of the compounds was determined at 80°C using Negretti Mooney Viscometer, Mark III according to ASTM D 1646-96a.

Measurement of rheological properties

The rheological properties of the compounds were studied using a Monsanto processibility tester (MPT, model no. 83077). The capillary used was 1 mm in diameter with a length/diameter (L/D) ratio of 30:1. No correction factor was applied to the data obtained from the rheometer since a capillary with a sufficiently high L/D ratio was used for the experiments. The multiple entry angles of 45° and 60° to the capillary minimized the pressure drop in the compounds while entering the capillary. Approximately 10–12 g of the test samples (depending on the density of the compositions) was taken in the heated barrel of the MPT and preheated for 5 min to obtain a uniform temperature distribution across the samples. Since the compounds were found undergoing curing inside the capillary at 120°C, a lower temperature of 80°C was employed for the processibility studies. The samples were pushed down through the barrel of the capillary rheometer using a plunger, which was heated to the same temperature as that of the barrel. In the present study, the rate of movement of the plunger through the capillary was adjusted in such a way that the samples, while extruding through the capillary, experienced apparent wall shear rate ($\dot{\gamma}_w$) from 12.27 s^{-1} to 110.47 s^{-1} with an increment in shear rate of 12.27 s^{-1}. The extrusion pressure was recorded using a transducer mounted in the barrel of the instrument, just above the entry to the die. The apparent shear stress (τ_w), apparent wall shear rate ($\dot{\gamma}_w$), and the apparent shear viscosity (η_w) were calculated using the following equations[23]:

$$\tau_w = \frac{\Delta P}{4\left(\frac{L_c}{D_c}\right)} \tag{1}$$

$$\dot{\gamma}_w = \frac{4Q}{\pi R^3} \tag{2}$$

$$\eta_w = \frac{\tau_w}{\dot{\gamma}_w} \tag{3}$$

where ΔP is the pressure drop along the length of the capillary; D_c and L_c are the diameter and length of the capillary, respectively; Q is the volumetric flow rate of the material within the capillary; and R is the radius of the capillary. The diameter of the extrudate, coming out of the capillary, was measured using a detector with a scanning He-Ne beam and the percentage of die swell is given by

$$\%\ \text{die swell} = \frac{100(D_e - D_c)}{D_c} \tag{4}$$

where D_e is the diameter of the extrudate.

Measurement of mechanical properties

The stress-strain properties of the cured samples were measured according to ASTM D 412-98A specification using dumb-bell test pieces in a Zwick Universal Testing Machine (UTM, model 1445) at a crosshead speed of 500 mm/min. In order to study the effect of fiber orientation on the physical properties of the composites, the samples with fibers oriented along the milling direction (longitudinal, denoted by L) and across the milling direction (transverse, denoted by T) were cut and the properties of the samples with both longitudinally and transversely oriented fibers were determined.

Measurement of dynamic mechanical properties

Test specimens having approximate dimension 30 mm × 10 mm × 2 mm with fiber orientation in the direction parallel to the longitudinal axis were tested under single cantilever bending mode at a frequency of 1 Hz and strain of 0.01%, using Rheometric Scientific DMTA IV at heating rate of 2°C/min. and temperature range −50°C to +30°C. The temperature corresponding to the peak in tan δ versus temperature plot was taken as the glass-to-rubber transition temperature, abbreviated as T_g.

Aging studies

Aging studies were performed by determining the mechanical properties after aging of the test specimens at 70°C for 48 h in a circulating air oven. Prior to testing, the aged samples were conditioned at room temperature for 24 h.

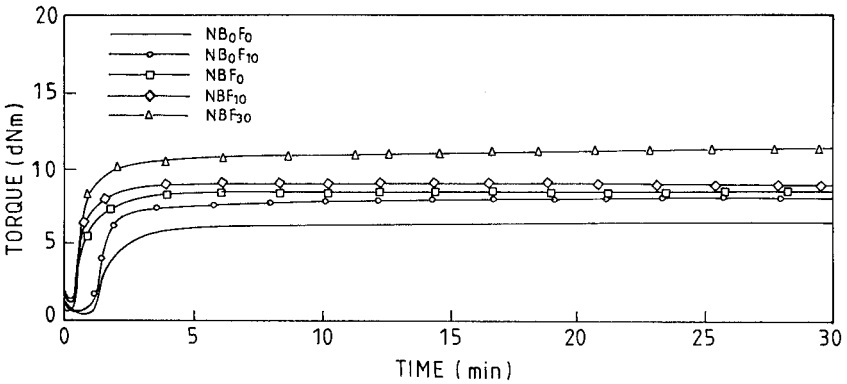

Figure 1 Monsanto rheographs of the compounds at 150°C.

SEM studies

The tensile fractured samples and the extrudate surfaces, obtained after extruding through the Monsanto processibility tester were studied by using JEOL scanning electron microscope (SEM, model JSM 5800). Prior to observation, the samples were sputter coated with gold in a vacuum evaporator. In order to study the extrudate surface morphology, samples having a length of 2 mm were used. The fiber orientation in the interior of the extrudate was studied by slicing the extrudate at room temperature using a sharp knife and the sliced portions were examined using SEM. All analyses were carried out within 48 h of the experiment.

Swelling studies

Rectangular specimens of dimension of 25 mm × 10 mm × 2 mm were used in the study. For the measurement of linear swelling ratio, which is the ratio of the dimension of the test specimen after swelling to the dimension before swelling, test pieces were cut with their long axis parallel to the direction of preferential orientation of fibers. Length, width, and thickness of the specimens were accurately measured before and after 48 h of immersion in butane-1-one at 30°C.

Measurement of hysteresis loss

Dumbbell shaped test pieces were cut in two directions: along the mill direction (longitudinal, denoted by L) and transverse (across the mill direction, denoted as T). The measurement of hysteresis at 50% elongation was carried out at 25°C using a Zwick Universal Testing Machine (UTM, model 1445) at a crosshead speed of 500 mm/min. The work done under the first stress-strain cycle was obtained by measuring the area under the loop.

AFM studies

The specimens for AFM studies were prepared by cryomicrotoming in a Reichert-Jung Ultracut Ultramicrotome, using glass knives (made using LKB Bromma 7800 Knife Maker), after freezing the specimens below its glass transition temperature using liquid nitrogen. Average sample thickness was 20 μm.. The AFM measurements were carried out in air at ambient conditions (25°C) using Dimension 3000 Atomic Force Microscope, manufactured by Digital Instruments (Santa Barbara, CA). Topographic images were recorded in the tapping mode. Scanning was done using etched silicone tips (TESP probe), each with a nominal tip radius of curvature of 5–10 nm and spring constant in

TABLE III
Processing Characteristics of the NBR-Melamine Fiber Compounds

Compositions	NB_0F_0	NB_0F_{10}	NBF_0	NBF_{10}	NBF_{20}	NBF_{30}
Resorcinol/hexamine/silica (phr)	0/0/0	0/0/0	10/6/5	10/6/5	10/6/5	10/6/5
Fiber (phr)	0	10	0	10	20	30
Rheometer maximum torque M_{II} at 150°C (dNm)	6.6	8.4	8.6	9.0	11.0	12.4
Rheometer minimum torque M_L at 150°C (dNm)	0.5	0.6	0.7	0.8	1.0	1.2
M_H-M_L, (dNm)	6.1	7.9	7.9	8.2	10.0	11.1
Rheometer optimum cure time, t_{90} (min)	4.4	5.1	2.4	1.8	1.8	2.0
Cure rate index (% min^{-1})	34.5	27.6	55.3	77.5	75.8	68.5
Mooney viscosity ML (1 + 4) 80°C	49	78	52	66	70	95
Mooney scorch time (min)	9.4	3.9	9.7	4.2	4.8	3.5

the range of 20–100 N/m. The cantilever was oscillated at its resonance frequency, which ranged between 200 and 400 kHz. The set point ratio of the cantilever, which governs the tapping force, was between 0.8 and 0.9 for all the scans. All the images were recorded using a free oscillation amplitude of 140±10. The general characteristics of the probes are: cantilever length, 125 μm; cantilever configuration, single beam; reflective coating, uncoated; side wall angles, 17° side, 25° front, 10° back. All the images contained 256 data points. Scanning was done in different data scales, ranging from 200 nm to 5 μm and the scan area was either 20 μm × 20 μm or 30 μm × 30 μ m. Data scale in AFM controls the vertical range of the images; the higher the data scale, the lower the image resolution will be. The images obtained after scanning the surfaces were analyzed using Nanoscope III-a software, version 4.

RESULTS AND DISCUSSION

Fiber breakage

Melamine fiber is in pulp form and the filaments have discontinuous length. The filament diameter is in the range 12–16 μm. Considerable fiber breakage has taken place during mixing of the fiber filled compounds. The average aspect ratio of the fibers after Brabender mixing is 250. The long filaments are further broken down into short filaments during mill mixing, and the fiber length varies between 0.08–0.25 mm after mill mixing. The average aspect ratio of the fiber after mill mixing is 10.

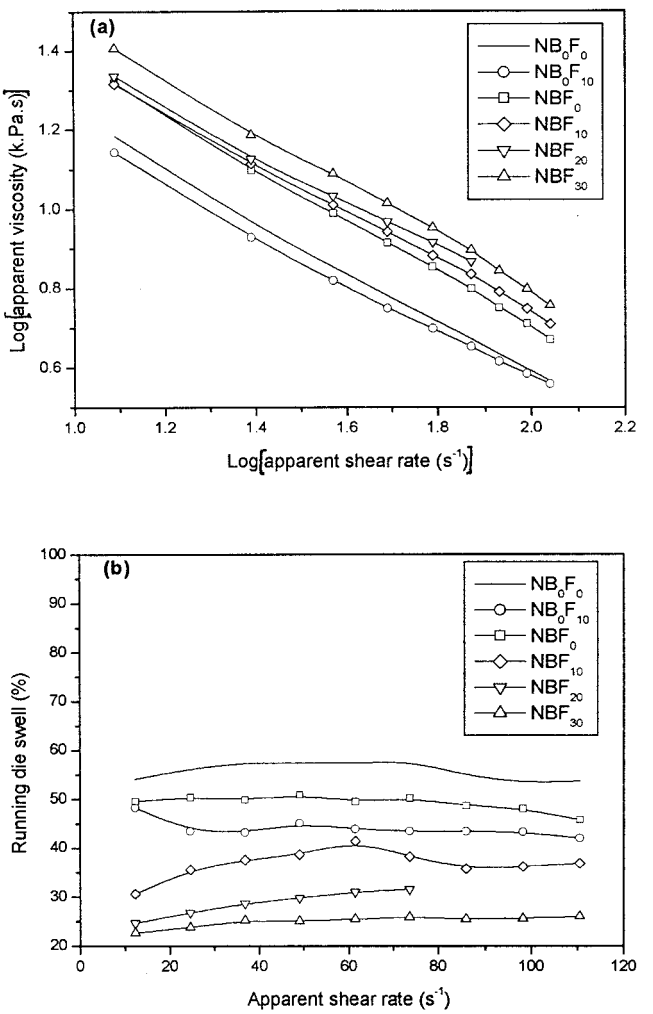

Figure 2 (a) Plots of log apparent viscosity versus log apparent shear rate; (b) Plots of running die swell versus apparent shear rate.

Processing characteristics and mechanical properties of the composites

Monsanto rheographs of the samples are given in Figure 1. The results of Monsanto Rheometric studies and Mooney viscosity measurements of the compounds are summarized in Table III. The following observations can be made from Table III: a) incorporation of melamine fiber and/or dry bonding system increases the rheometer minimum and maximum torques; b) incorporation of melamine fiber alone into the NBR matrix (that is, compound NB_0F_{10}) decreases the Mooney scorch time and also the cure rate index with an increase in the optimum cure time; c) incorporation of the dry bonding system alone into the NBR matrix (that is, compound NBF_0) causes no significant change in the Mooney scorch time but the cure rate index is increased and the rheometer optimum cure time is decreased; d) when both fiber and dry bonding system are present together in the matrix (that is, compounds NBF_{10}, NBF_{20}, and NBF_{30}), the Mooney scorch time is decreased, the cure rate index is increased, and the rheometer optimum cure time is decreased compared with the unfilled NBR compound (that is, compound NB_0F_0). Incorporation of melamine fiber alone into the NBR matrix increases the Mooney viscosity of the compound. However, resorcinol present in the dry bonding system plasticizes the NBR matrix, which makes Mooney viscosity of the compound NBF_{10} lower than that of NB_0F_{10}. The marginal increase in Mooney viscosity of the compound NBF_0 compared with that of NB_0F_0 is due to the presence of silica in the dry bonding system. Presence of dry bonding system increases the cure rate of the compounds. The role of the dry bonding system on the cure behavior of the short-fiber rubber composites has been reported.[4,24] The amine groups in the dry bonding system (due to the presence of hexamine) accelerate the curing process whereby the cure rate is increased and the optimum cure time is decreased in the presence of the dry bonding system. When the fiber and the dry bonding system are present together in the matrix, there is an increase in the cure rate and

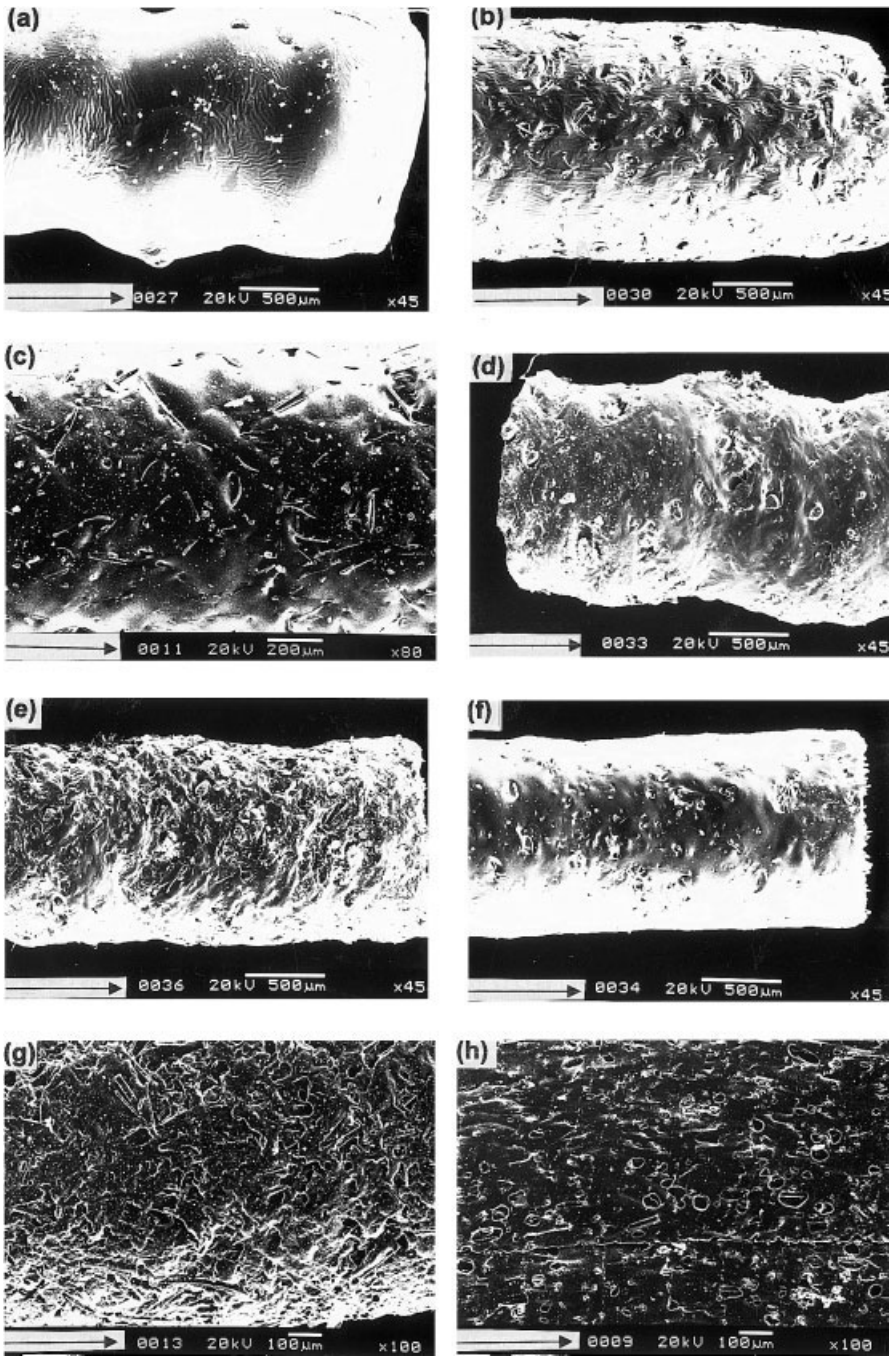

Figure 3 SEM photomicrographs of the extrudates: (a) NB_0F_0 at a magnification of ×45; (b) NB_0F_{10} at a magnification of ×45; (c) NB_0F_{10} at a magnification of ×80; (d) NBF_0 at a magnification of ×45; (e) and (f) NBF_{10} at a magnification of ×45; (g) and (h) NBF_{30} at a magnification of ×100. Figures 3(a) to 3(e), 3(g) and 3(h) are at a shear rate of 98.2 s^{-1} and figure 3(f) is at a shear rate of 49.1s-1. Figures 3(a) to 3(e) are for the extrudate surface while figure 3(h) is the interior of the extrudate. The arrows indicate direction of the major axis of the extrudates.

decrease in the optimum cure time with respect to the compound containing either fiber or dry bonding system alone (compound NBF_{10} vis-à-vis compounds NB_0F_{10} or NBF_0). The cure rate decreases with increase in fiber loading.

The rheological characteristics of the compounds are shown in Figure 2. It is evident from Figure 2a that all the compounds show pseudoplasticity in the shear rate region employed. The apparent capillary viscosity of the compound NB_0F_{10} is lower than that of the unfilled compound. The wall slippage due to the presence of fibers on the extrudate surface[25] may be the reason for the decrease in viscosity of the compound NB_0F_{10}. Presence of fibers on the extrudate surface is visible in the SEM photomicrograph of the extrudate surface of the compound NB_0F_{10} (Figs. 3b and 3c).

TABLE IV
Physical Properties of the NBR-Melamine Fiber Composites[a]

Compositions		NB_0F_0	NB_0F_{10}	NBF_0	NBF_{10}	NBF_{20}	NBF_{30}
Resorcinol/hexamine/silica (phr)		0/0/0	0/0/0	10/6/5	10/6/5	10/6/5	10/6/5
Fiber (phr)		0	10	0	10	20	30
Young's modulus (MPa)	L[b]	1.6 (1.8)	2.4 (3.7)	2.6 (3.1)	4.8 (4.8)	5.8 (6.1)	9.6 (11.3)
	T[b]	1.6 (1.8)	2.2 (3.5)	2.6 (3.1)	3.9 (4.2)	4.5 (5.7)	6.8 (7.2)
Tensile strength (MPa)	L	1.8 (2.3)	2.4 (2.5)	8.1 (6.3)	10.6 (10.7)	8.1 (9.9)	8.0 (8.9)
	T	1.8 (2.3)	2.4 (2.6)	8.1 (6.3)	9.8 (10.0)	8.1 (8.1)	7.6 (8.4)
Elongation at break (%)	L	335 (296)	388 (222)	359 (299)	416 (300)	230 (157)	269 (183)
	T	335 (296)	413 (248)	359 (299)	421 (302)	277 (195)	323 (220)
Stress at 100% elongation (MPa)	L	1.0 (1.1)	1.2 (1.4)	1.6 (2.0)	3.6 (3.3)	5.6 (7.7)	6.7 (8.0)
	T	1.0 (1.1)	1.1 (1.3)	1.6 (2.0)	3.2 (3.3)	4.1 (5.1)	3.5 (4.2)
Hysteresis loss, first cycle, ($\times 10^{-3}$)(J/m^2)	L	4 (3)	17 (15)	9 (9)	21 (28)	46 (59)	116 (122)
	T	4 (3)	18 (23)	9 (9)	20 (27)	41 (52)	60 (83)
Hardness (shore A)		46 (48)	51 (52)	56 (58)	62 (64)	68 (75)	74 (77)
Swelling ratio	L	1.61 (1.60)	1.54 (1.47)	1.50 (1.47)	1.37 (1.33)	1.25 (1.13)	1.20 (1.13)
	T	1.61 (1.60)	1.57 (1.50)	1.50 (1.47)	1.42 (1.30)	1.39 (1.30)	1.30 (1.28)

[a] Values in the parentheses indicate properties determined after aging the composites in a circulating air aging oven at 70°C for 48 h.
[b] L = properties determined with test specimen cut in the direction parallel to the milling direction (longitudinal direction); T = properties determined with test specimen cut in the direction perpendicular to the milling direction (transverse direction).

Presence of the dry bonding system in the NBR matrix increases the apparent viscosity and the incorporation of the fiber to the compound containing the dry bonding system causes a progressive increase in apparent viscosity. The effect of the fiber in increasing the apparent viscosity of the compound is prominent in the higher shear rate region of the capillary viscometer where there is a significant difference between the viscosities of the compounds. Similar observation has been reported in the case of maleated EPDM-melamine fiber composites.[10]

As expected, the die swell of the fiber filled compounds is lower than that of the compounds containing no fiber (Fig. 2b). Incorporation of either the dry bonding system or the fiber reduces the die swell. However, the reduction in die swell is most pronounced when the matrix is filled with both dry bonding system and melamine fiber. Die swell is reduced with increase in fiber loading. The changes in the extrudate surface morphology with the incorporation of the dry bonding system and/or melamine fiber are shown in the SEM photomicrographs of the extrudate surfaces of the compounds, given in Figures 3a to 3e, at a shear rate of 98.2 s^{-1}. It is evident that the incorporation of melamine fiber considerably reduces the extrudate distortion of the unfilled compound (Fig. 3a vis-à-vis Fig. 3b). However, presence of the dry bonding system in the matrix helps in achieving a smoother extrudate (Figs. 3d and 3e). Comparison of extrudate surface of the compound NBF_{10} at two different shear rates (98.2 s^{-1} and 49.1 s^{-1}, that is, Figs. 3e and 3f respectively) shows that a smoother extrudate is obtained at a lower shear rate of 49.1 s^{-1}.

The extrusion of the compounds through the capillary causes further fiber breakage. Fiber aspect ratio is reduced to 7 after extrusion. It is also observed that the fiber orientation is random on the extrudate surface, whereas the fibers are more oriented inside the extrudate (Figs. 3g and 3h respectively). In addition, fibers are visible on the surface of the extrudate (Figs. 3b, 3c, and 3g). As already explained, the fibers on the surface of the extrudate cause wall slippage whereby the viscosity is reduced.[25,26] However, for the compounds containing the dry bonding system, due to the coating of the fiber surface by the matrix (Fig. 3g), the wall slippage is reduced and viscosity is increased, especially at higher fiber loading.

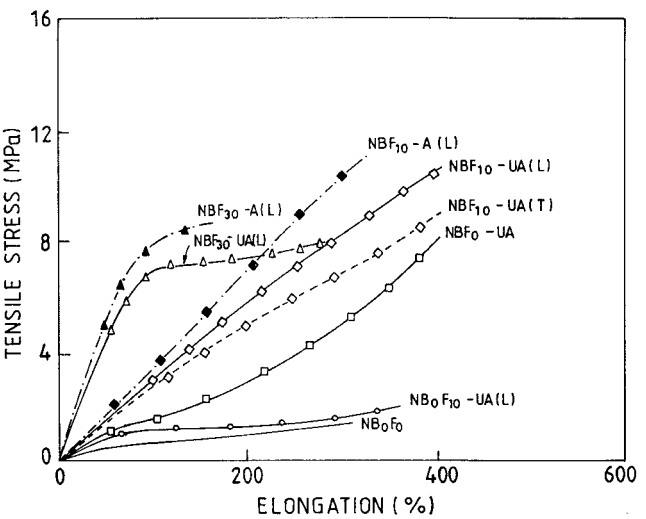

Figure 4 Stress-strain curves of the unaged and aged (at 70°C for 48 h) composites with varying fiber loadings. UA, unaged; A, aged composites; L, specimens cut in the direction parallel to the milling direction; T, specimens cut in the direction perpendicular to milling direction.

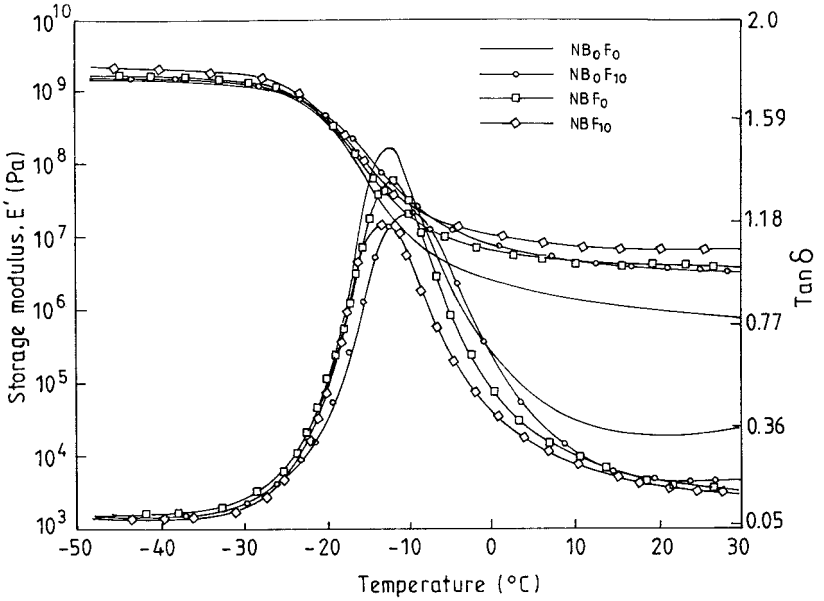

Figure 5 Plots of storage modulus and tan δ versus temperature of the composites. Test specimens cut with longitudinal axis parallel to the milling direction

Mechanical properties (Table IV) and the stress-strain curves (Fig. 4) show that there is a marginal increase in tensile strength and modulus with the incorporation of melamine fiber in the matrix. However, the properties are improved considerably in the presence of the dry bonding system. For example, there is more than a twofold increase in tensile strength and modulus with the incorporation of the dry bonding system (that is, composites NB_0F_{10} vis-à-vis NBF_{10}) with a consequent decrease in linear swelling ratio, which can be used as a measure of the interfacial adhesion between the fiber and the matrix.[27] Therefore, it can be postulated that the dry bonding system consisting of resorcinol, hexamine, and silica can be used in NBR-melamine fiber composites for improving the interfacial adhesion between the fiber and the matrix. A higher concentration of the fiber (beyond 10 phr) does not cause significant increase in the tensile strength of the composite though modulus and hardness are increased, followed by a reduction in linear swelling ratio. The anisotropy in mechanical properties and swelling characteristics are evident in all the fiber loadings. Increase in the fiber loading increases the hysteresis of the composites. A higher fiber loading (30 phr) causes significant increase in hysteresis and the anisotropy in hysteresis is more evident here. On comparing the hysteresis of the composites NB_0F_{10} with that of the compound NBF_0, it can be seen that the presence of fiber contributes more to the hysteresis than the presence of the dry bonding system. Aging at a lower temperature (70°C for 48 h) does not cause significant improvement in mechanical properties, though there is a marginal increase in tensile strength and modulus of the fiber-rubber composites due to aging, especially in the presence of the dry bonding system. However, aging causes a reduction in linear swelling ratio and elongation at break. Aging of the composites increases the hysteresis, as shown in Table IV. Hysteresis of the aged composites also increases with increase in fiber loading. From Table IV, it can be concluded that the composite properties, especially tensile strength, is lowered beyond 10 phr fiber loading. In addition, at higher fiber loadings, the composites become stiffer with a fall in elongation at break. Therefore, studies on the fiber-matrix adhesion based on dynamic mechanical properties, SEM, and AFM have been made with the composites NB_0F_{10} and NBF_{10}.

Figure 5 shows the effect of the dry bonding system on the dynamic mechanical properties of the composites, determined with test specimens cut in the direction parallel to the milling direction (longitudinal direction). The results of the dynamic mechanical mea-

TABLE V
Dynamic Mechanical Properties of the NBR-Melamine Fiber Composites[a]

Compound	T_g (°C)	Tanδ at T_g	Storage Modulus at T_g (MPa)	Storage Modulus at 30°C (MPa)
NB_0F_0	−12.1	1.5	18.9	0.8
NB_0F_{10}	−10.7	1.2	43.2	3.5
NBF_0	−12.4	1.4	43.0	3.9
NBF_{10}	−13.0	1.2	56.8	6.8

[a] Properties determined with test specimens cut in the direction parallel to the milling direction (longitudinal direction).

surements are tabulated in Table V. The role of the dry boding system in improving the fiber-matrix adhesion is evident on comparing the loss modulus and tan δ curves of the composites NB_0F_{10} and NBF_{10}. Among the four compounds studied, the highest dynamic modulus and the lowest tan δ are shown by the composite NBF_{10}. It can also be noted that when only fiber is present in the matrix, (composite NB_0F_{10}), there is a positive shift in tan δ peak temperature. Moreover, fiber causes greater reduction in tan δ peak height than the dry bonding system. This shows that there is a strong fiber-rubber bonding (even in the absence of the dry bonding system), which is, however, facilitated by the dry bonding system. This fiber-rubber bonding may be the reason for the high Mooney viscosity and low Mooney scorch time of the compound NB_0F_{10}, as explained earlier (Table III). Accordingly, the storage modulus (E′) at T_g follows the order $NBF_0 < NB_0F_{10} < NBF_{10}$ (Table V).

The role of the dry bonding system in improving the adhesion between the fiber and the matrix is evident in the SEM photomicrographs (Fig. 6). Figure 6a is the SEM photomicrograph of the tensile fracture surface of the composite NB_0F_{10}, which contains no dry bonding system. The smooth fracture surface and debonding of the fibers from the matrix show weak adhesion between the fibers and the matrix. However, when the dry bonding system is present, the morphology of the fracture surface is changed with fracture occurring in more than one plane (Fig. 6b, composite NBF_{10}). It is evident that the fracture surface is rough compared with that of the composite NB_0F_{10} and the failure mode involves fiber breakage rather than fiber pullout. The strong attachment of the fibers on the matrix is visible here. The preferential orientation of the fibers in the milling direction is also evident in the SEM photomicrographs. Figures 6a and 6b are the SEM photomicrographs of the tensile fracture surfaces with fiber orientation in the direction parallel to the milling direction (longitudinal direction, denoted by L). Here fibers are protruding from the fracture surface, confirming that there is an orientation of fibers in the milling direction. Figure 6c is the SEM photomicrograph of the tensile fracture surface of the composite NBF_{10} with test specimen cut in the direction perpendicular to the milling direction (transverse direction, denoted by T). Here fibers are seen mostly lying parallel to the fracture surface, again indicating that the preferential orientation of the fibers is in the opposite direction, that is, parallel to the milling direction). It can also be noted from Table IV and Figure 6 that the anisotropic behavior is pronounced only when there is a good adhesion between the fiber and the matrix. A more random orientation of the fibers is observed in the case of NB_0F_{10}, which contains no dry bonding system (Fig. 6a).

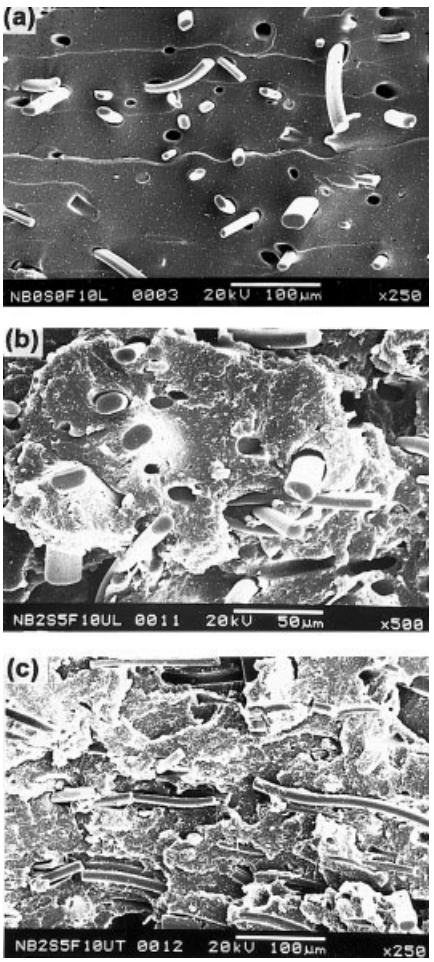

Figure 6 SEM photomicrographs of the tensile fracture surfaces of the composites: (a) composite NB_0F_{10} with test specimen cut in the direction parallel to the milling direction (longitudinal direction, denoted by L); (b) composite NBF_{10} with test specimen cut in the direction parallel to the milling direction; (c) composite NBF_{10} with test specimen cut in the direction perpendicular to the milling direction (transverse direction, denoted by T).

AFM studies

Incorporation of the dry bonding system into the NBR matrix causes morphological changes on the matrix surface and the fiber-matrix interphase of the composites. Figures 7a to 7d are the AFM surface plots of the matrix phase of the compositions NB_0F_0, NB_0F_{10}, NBF_0, and NBF_{10} respectively. The matrix surface morphology of the compositions, which contain no dry bonding system (that is, compositions NB_0F_0 and NB_0F_{10}), are almost similar and are different from that of the compounds that contain the dry bonding system (that is, compositions NBF_0 and NBF_{10}). Constituents of the dry bonding system causes formation of a large number of granules on the matrix surface, which are aggregated particles, especially silica, which is a part of the dry bonding system.

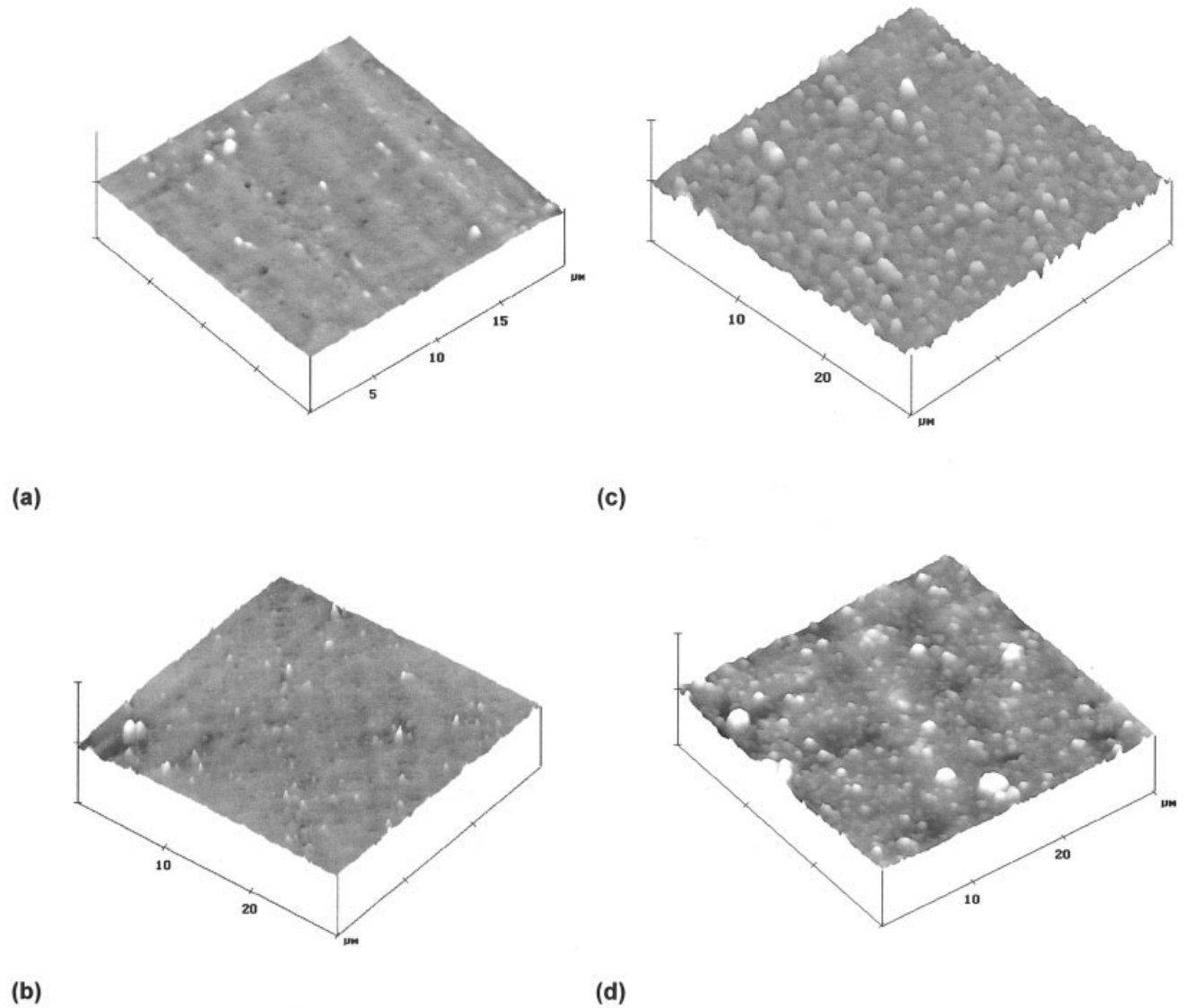

Figure 7 AFM surface plots of the matrix phase of the composites in a data scale of 3000 nm: (a) compound NB_0F_0; (b) composite NB_0F_{10}; (c) compound NBF_0; (d) composite NBF_{10}.

In short fiber-rubber composites, if the fibers are not bonded properly with the rubber matrix, fibers slide past each other under tension deforming the matrix and thereby reducing the strength properties.[4] Here, loads are not directly applied to the fibers, but are applied to the matrix. To obtain a high-performance composite, the load must be effectively transferred to the fibers, which is possible only when the fiber-matrix interphase is sufficiently strong. In addition, the adhesion between the fiber and the matrix should be such that the failure occurs in the matrix rather than at the interphase. Though the mechanism of load transfer is not clearly understood, in the case of short fiber-rubber composites, it may take place through shear at the fiber-matrix interphase. The formation of an interphase between the fiber and the matrix with the incorporation of dry bonding system was observed by Rajeev et.al.[9,10,19] in the AFM images of melamine fiber reinforced EPDM and maleated EPDM rubber composites. On comparing the AFM surface plots of the composites NB_0F_{10} and NBF_{10} (Figs. 8a and 8b), it can be seen that in the presence of the dry bonding system, there is a strong interfacial adhesion between the fiber and the matrix, which is further evident in Figure 8c, at a higher resolution (lower data scale). The AFM section analysis of the composites NB_0F_{10} and NBF_{10} can be used to quantify the interphase formation. Figure 8d is the representative figure showing the section analysis of the composite NB_0F_{10}. In the absence of the dry bonding system, the average value of the width of the interphase between the fiber and the matrix (measured on five images, given in Table VI) is only 0.86 μm,

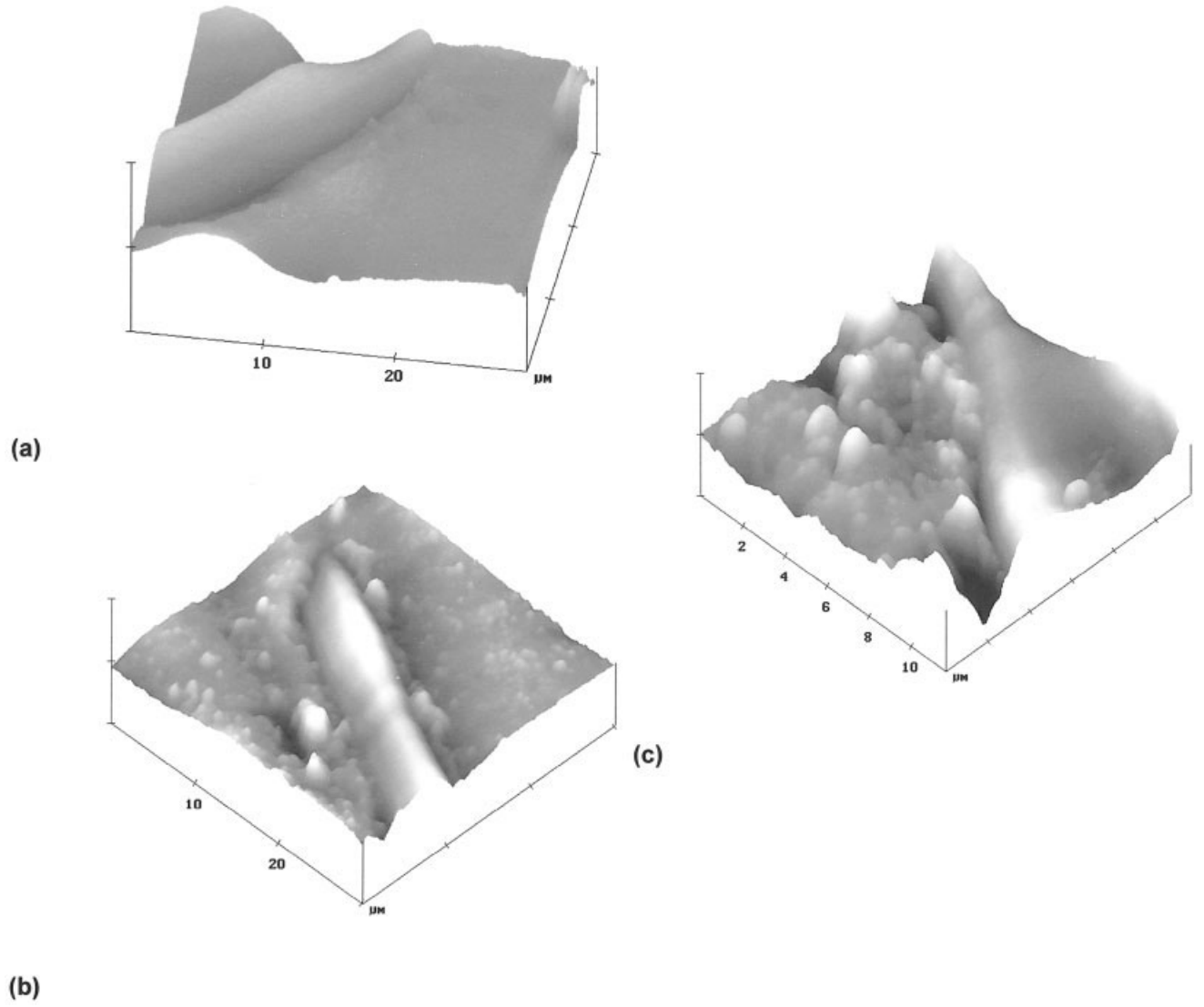

Figure 8 (a) AFM surface plot of the composite NB_0F_{10} in a data scale of 3000 nm. In the absence of the dry bonding system, width of the interphase is very low; (b) AFM surface plot of the composite NBF_{10} in data scale of 3000 nm. Incorporation of the dry bonding system causes formation of a well defined interphase between the fiber and the matrix; (c) AFM surface plot of the composite NBF_{10} in data scale of 1000 nm. At a smaller data scale, the attachment of the fiber to the matrix is clearer; (d) AFM section analysis of the composite NB_0F_{10}. Width of the interphase is shown by arrows; (e) AFM section analysis of the composite NBF_{10}. Width of the interphase (shown by arrows) is increased when dry bonding system is present in the matrix.

whereas incorporation of the dry bonding system (composite NBF_{10}, in Fig. 8e) causes an increase in the interphase width to 1.86 μm.

Mechanical properties, given in Table IV, show that aging of the composites at 70°C for 48 h causes marginal increase in tensile strength and modulus with a reduction in the elongation at break. The swelling restriction is also increased due to aging. AFM surface plots of the aged composites NB_0F_{10} and NBF_{10}, given in Figures 9a and 9b, respectively, in a data scale of 3000 nm, show that aging causes improved fiber-matrix attachment in the presence of the dry bonding system. The width of the interphase is increased to 2.96 μm due to aging for the composite NBF_{10}. This may be the reason for the increase in mechanical properties and swelling restriction of the aged composites,

TABLE VI
Interphase Thickness of the Composites[a]

Composition	Interphase Thickness[b] (μm)
NB_0F_{10}	0.86 (1.09)
NBF_{10}	1.86 (2.96)

[a] Values are the average of 5 measurements.
[b] Values in the parentheses are for the composites aged at 70°C for 48 h.

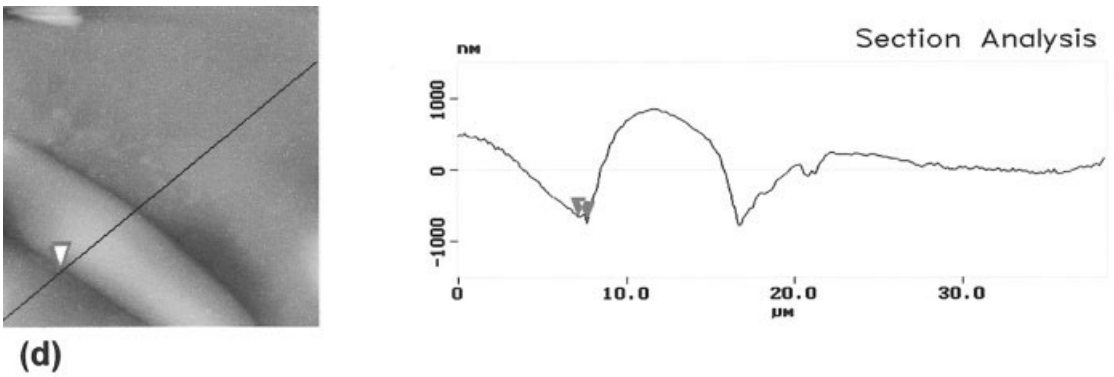

(d)

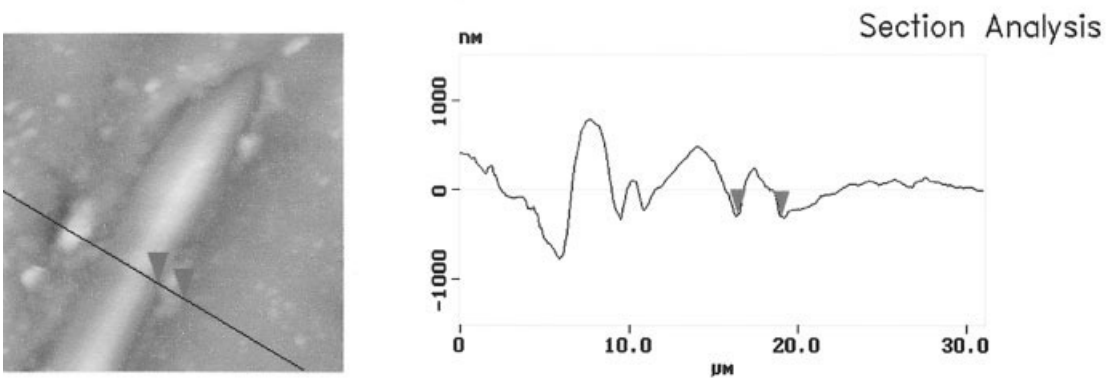

(e)

Figure 8 (*Continued from the previous page*)

especially in the presence of the dry bonding system. The width of the interphase of the composite NB_0F_{10}, which contains no dry bonding system, is increased marginally due to aging, as given in Table VI. Consequently there is a minor increase in the tensile strength and modulus of the composite NB_0F_{10} due to aging. The AFM section analysis of the aged composites, given in Figures 9c and 9d show the effect of aging on the fiber-matrix interphase. The irregular trace line from one half of the fiber surface (shown by arrows) is due to the matrix coverage on the fiber surface. The marginal increase in interphase thickness due to aging of the composite NB_0F_{10} is evident in Figure 9c.

CONCLUSIONS

Dry bonding system comprised of resorcinol, hexamethylene tetramine, and silica causes significant improvement in the mechanical properties of the NBR-melamine fiber composites. In the presence of the dry bonding system, tensile strength and elongation at break are increased, followed by a reduction in solvent swelling characteristics, which shows that the interfacial adhesion between the fiber and matrix is improved. Dynamic mechanical studies also confirm the role of the dry bonding system in improving the interfacial adhesion between the fiber and the matrix.

Presence of fiber or dry bonding system in the compound reduces the extrudate swell of the compounds. Extrusion through the capillary causes further fiber breakage with a reduction in fiber aspect ratio from 10 (after mill mixing) to 7 (after extrusion). Fiber orientation is random on the extrudate surface whereas fibers are more oriented in the interior of the extrudate.

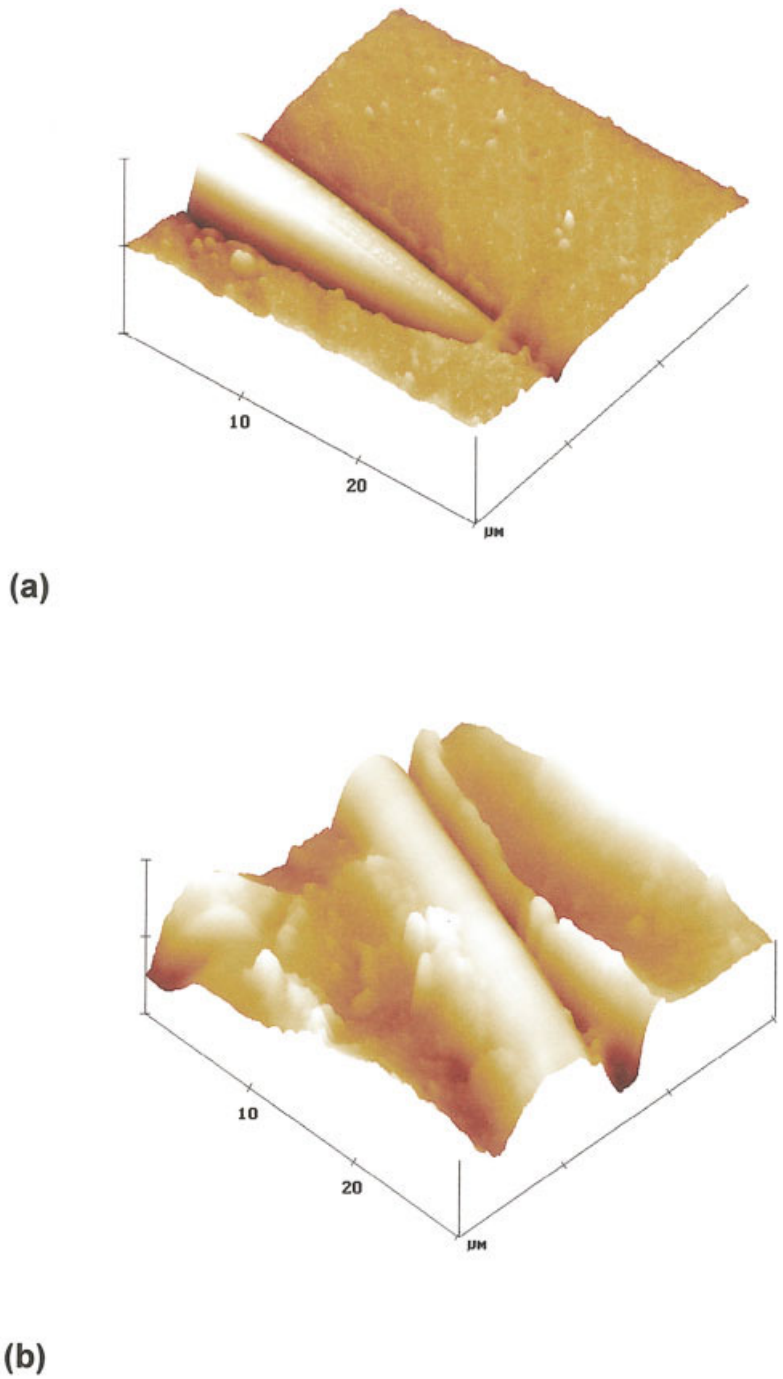

Figure 9 (a) AFM surface plot of the aged composite NB_0F_{10} in a data scale of 4000 nm. In the absence of the dry bonding system, the matrix surface and fiber surface are relatively smooth; (b) AFM surface plot of the aged composite NBF_{10} in a data scale of 3000 nm. Presence of the dry bonding system causes the matrix to cover the fiber surface due to aging; (c) AFM section analysis of the aged composite NB_0F_{10}. Width of the interphase is marginally increased due to aging; (d) AFM section analysis of the aged composite NBF_{10}. Arrows in the right hand side of the image show coverage of the fiber surface by the matrix.

Composites display anisotropy in mechanical properties due to the preferential orientation of melamine fibers in the milling direction, which is pronounced at higher fiber loading. The SEM images of the tensile fracture surfaces show the preferential orientation of the fibers along the milling direction.

SEM and AFM images show that the presence of the dry bonding system in the matrix causes the formation of an interphase between the fiber and the matrix. The strong attachment of the fiber to the matrix in the presence of the dry bonding system is evident in the SEM photomicrographs of the tensile fracture surfaces

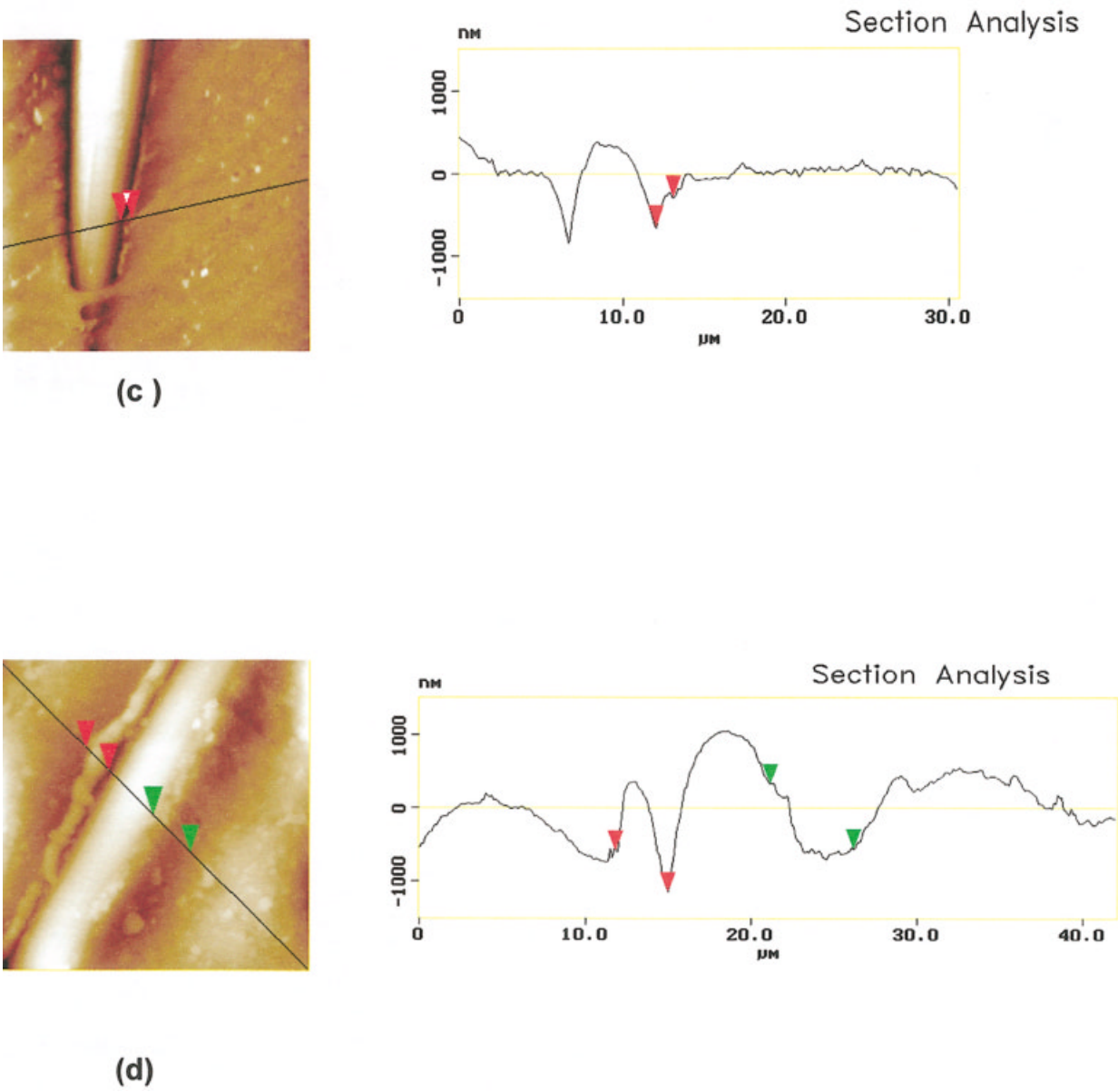

Figure 9 (*Continued from the previous page*)

of the composites. AFM surface plots of the microtomed surfaces confirm the above observation.

AFM section analyses show that in the presence of the dry bonding system the width of the interphase between the fiber and the matrix is increased from 0.86 μm to 1.86 μm. The formation of this well-defined interphase in the presence of the dry bonding system may be the reason for the improved mechanical properties of the composites.

Aging of the composite at 70°C for 48 h causes an increase in the tensile strength and modulus and swelling restriction, especially in the presence of the dry bonding system. The improved fiber-matrix attachment due to aging, which is evident in the AFM section analysis of the aged composite containing the dry bonding system, may be the reason for this improvement in properties.

The authors thank Indian Space Research Organization, Bangalore for the financial assistance and M/s BASF South East Asia Pte Ltd, Singapore for the free supply of melamine fiber. Rajeev R.S acknowledges the financial support provided by the Australia-India Council, Canberra for doing some of the experiments (Atomic Force Microscopy) in the University of New South Wales, Sydney, Australia.

References

1. Foldi, A. P. In Short Fiber Polymer Composites; De, S. K.; White, R., Eds.; Woodhead Publishing Limited: Cambridge, England, 1996; Chapter 9.

2. Van Hattum, F. W. J.; Bernardo, C. A. Polym Compos 1999, 20, 524.
3. Goettler, L. A.; Shen, K. S. Rubb Chem Technol 1983, 56, 619.
4. Murty, V. M.; De, S. K. Polym Eng Revs 1984, 4, 313.
5. Setua, D. K.; De, S. K. J Mat Sci 1984, 19, 983.
6. Saikrasun, S.; Amornsakachai, T.; Sirisihna, C.; Meesiri, W.; Bualek-Limcharoen, S. Polymer, 1999, 40, 6437.
7. Hopen, T. J. Microscope, 2000, 48, 107.
8. Technical literature, Basofil fiber, BASF Corporation, Enka, NC, USA, 1999.
9. Rajeev, R. S.; Kao, G. J. P.; Bandyopadhyay, S.; Bhowmick, A. K.; De, S. K. Polym Comp 2002, 23, 574.
10. Rajeev, R. S.; Bandyopadhyay, S.; Bhowmick, A. K.; De, S. K. J Appl Polym Sci 2003, 89, 1211.
11. Goritz, D.; Raab, H.; Frohlich, J.; Maier, P. G. Rubb Chem Technol 1999, 72, 929.
12. Tsukruk, V. V. Rubb Chem Technol 1997, 70, 430.
13. Ghosh, S.; Khastgir, D.; Kao, G. J. P.; Kok, L.; Bandyopahdyay, S.; Bhowmick, A. K. J Mater Sci Lett 2000, 19, 2161.
14. Hautojarvi, J.; Leijala, A. J Appl Polym Sci 1999, 74, 1242.
15. Rebouillat, S.; Peng, J. C. M.; Donnet, J. B. Polymer 1999, 40, 7341.
16. Trifonova-Van Haeringen, D.; Schonherr, H.; Vancso, G. J.; Van Der Does, L.; Noordermeer, J. W. M.; Janssen, P. J. P. Rubb Chem Technol 1999, 72, 862.
17. Ganter, M.; Brandsch, R.; Thomann, Y.; Malner, T.; Bar, G. Kautsch Gum Kunst 1999, 52, 717.
18. Mass, S.; Lay, R.; Gronski, W. Kautsch Gum Kunst 1996, 49, 166.
19. Rajeev, R. S.; Kao, G. J. P.; Bandyopadhyay, S.; Bhowmick, A. K.; De, S. K. J Mater Sci 2001, 36, 2621.
20. Ibarra, L. Kautsch Gum Kunstst 1994, 47, 578.
21. Akhtar, S.; De, P. P; De, S. K. J Appl Polym Sci 1986, 32,5123.
22. Derringer, G. C. J Elastoplast 1971, 3, 230.
23. Brydson, J. A. Flow Properties of Polymer Melts, 2nd ed.; George Godwin, London, 1981.
24. Ramayya, A. P.; Chakraborty, S. K.; De, S. K. J Appl Polym Sci 1984, 29, 1911.
25. Worth, R. A.; Parnally, J.; Helmy, H. A. A. Polym Eng Sci 1977, 17, 257.
26. Roy, D.; Gupta, B. R. J Appl Poly Sci 1993, 49, 1475.
27. Ibarra, L.; Chamorro, C. J Appl Polym Sci 1991, 43, 1805.